Proceedings of the
Annual Stability Conference
Structural Stability Research Council
San Antonio, Texas, March 19-22, 2024

Stability of a deployable awns on a compliant steel geosystem for nonlinear soil-structure interaction

Ann C. Sychterz[1]

Abstract

Compliant geosystems undergo shape changes through deformation provides a novel solution addressing tensile capacity while minimizing material. Deployable fins, called awns, along the circumference of the geosystem unfold from the geosystem, increasing the region of soil engaged and surface area for tensile resistance. However, tensile capacity controls the size of the piles and stability within the soil medium has not yet been studied. In traditional design, piles are often quite large to account for these forces, leading to high material and energy use. Analysis of the joint of deployable awns and their limit of deployment due to stability of the thin plate-like structures underground requires soil-structure interaction that has not yet been studied. This paper presents the fundamental analysis and discussion of the stability of the thin-shell awns along the surface of the geosystem using form-finding of the steel deployable compliant geosystem. The goal of this work is to develop an analytical model to show the deformation limitations versus increased tensile capacity of geosystems through geometrically nonlinear shape changes and compare with experimental results of small-scale prototypes.

1. Introduction

A deployable compliant geosystem, as described in this paper, applies principles of shape-changing structures to improve the performance of ground anchors. Improving the performance of foundation systems will reduce the amount of material associated with them, addressing more sustainable practices in geotechnical engineering. Less material facilitates logistics and fuel associated with transportation as units can be more efficiently moved to remote installation locations offshore or on land. Additionally reduced are the energy associated with the system and its cost.

Deployable structures are a type of transformable structure that change shape from a compact state to an expanded state as their size increases (Pellegrino, 2001; Akgun et al., 2011). Deployable structures have potential for increased capacity and the ability to be stored in a smaller volume. In practice, many contemporary structures including scissor structures (Akgun et al., 2022; Garcia-Mora and Sanchez-Sanchez, 2021) use rigid materials and preconnected parts for easier

[1] Assistant Professor, University of Illinois Urbana-Champaign, <asychter@illinois.edu>

deployment. Flexible materials are often seen in single-use deployable structures for space applications such as solar sails, solar arrays, and deployable spacecraft (Furuya, 1992; Tibert 2002; Block et al., 2011). A combination of rigid and flexible materials used in deployable structures can be seen in examples like deployable masts with flexible cables (Tibert and Pellegrino 2003) and membrane-based space reflectors (Datashvili, 2010). Use of deployable structures has been limited to aboveground and space structures but has not yet been expanded to underground use.

Compliant structures change shape via plastic deformations, where stability of these structures comes from the soil containment around the geosystem. Compliant elements are singular elements that deform to perform their functions (Howell et al., 2013). The mechanisms involved in these structures function without joints and are flexible like natural elements (Kota et al., 2001). While most structures are designed to be stiff and strong, the goal of compliant structures is to be flexible and strong, like those found in nature (Kota and Ananthasuresh, 1995; Frecker, 2013). Compliant mechanisms are advantageous because there is little assembly or pre-connection required, as singular elements are used (Zentner and Bohm, 2009). This can facilitate constructability and installation. Additionally, compliant mechanisms have low weight, which can decrease transportation requirements (Kota and Ananthasuresh, 1995; Howell, 2013). While previous work has looked to nature for inspiration, this work has mainly focused on aboveground applications.
Ground anchoring systems—including pile anchors—are underground foundation elements. These systems must resist compression due to gravity loads and tension due to friction. Piles can withstand a wide variety of load conditions but drawbacks include their performance under horizontal loading (Aubeny, 2017), environmental effects (Colaco, 2021), and cost (Audeny, 2017). Despite these drawbacks, anchor piles are an advantageous system for foundations due to their versatility.

Existing work has been done in combining radial protrusions with underground geosystems and in exploring systems that actively change shape during installation or operation. Helical piles, which are comprised of a pile with attached helical plates resist lateral and axial loads (Aubeny, 2017; Prasad and Rao, 1996). Static radial fins can also be installed in driven piles to better resist uplift loads when installed in sand (Tom et al., 2017). Suction embedded plate anchors are a system that deploys into soil after installation (Aubeny 2017; Wilde et al., 2001). Piles that have anchor wings have also been explored. After a pile is rotated into sand, wings hinge outward into sand and provide improved resistance to uplift loads (Sakr et al., 2020). The combination of deployable and compliant systems—the latter of which changes shape and size elastically—has not yet been explored for stability within geotechnical engineering.

Both deployable and compliant structures are seen in the internal structures of plants and animals (Pellegrino, 2001; Lienhard et al., 2015). Often, natural structures have inherent flexibility and softness, like in unravelling leaves and blooming flowers (Vincent, 2003). In structural engineering, the folding mechanisms associated with leaves, petals, and insect wings have been modeled and applied in large-scale origami structures (Baerlecken, 2014). In these models, the folds are joints and act like hinges. Here, a deployable compliant system is used as a precedent, but the compliant nature of the system is not preserved in the final model. Large scale structural analogues of these natural structures have not yet been developed.

The authors have previously developed a biologically inspired deployable compliant structure for geotechnical use. This system is inspired by the deployment of cheatgrass seeds and is comprised of a static pile with deployable shell-like compliant attachments, called awns, that deform away from the pile. From this work, geometry of the awns was shown to affect shear resistance (Sychterz et al., 2021). Noise pollution from hammer-driven piles and damage to surrounding foundations could be damaging contextual effects of this installation method. Although a preliminary design has been created (Tucker and Sychterz, 2022) this geosystem has not yet been experimentally tested to torque-driven piles. The objective of this paper is to develop an analytical model to show the deformation limitations versus increased tensile capacity of geosystems through geometrically nonlinear shape changes in-plane and out-of-plane to compare with experimental testing of small-scale prototypes.

2. Structure Description

This research focuses on a geosystem that is comprised of a cylindrical pile and several compliant attachments (Fig. 1). The scope of this paper is studying deployment during installation and in-service loading is not within this scope. Additionally, this work presents a solution to help with tensile forces that tend to be specific to the structure. The shell-like attachments – called awns – are radially arranged around the pile.

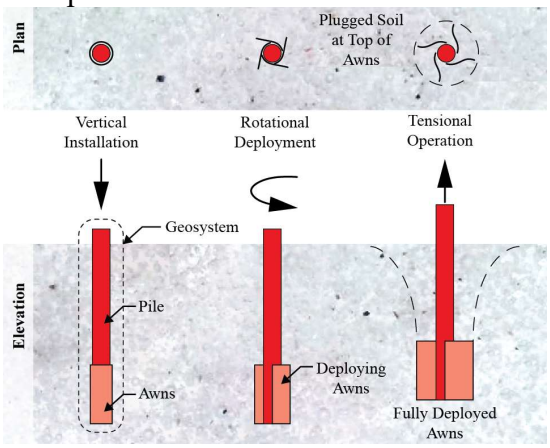

Figure 1: *Schematic illustration of deployable steel geosystem before, during, and after deployment.*

When the pile is rotated, the awns deploy into soil. This work presents deployable structures in sand. Due to their compliant nature, the awns deploy via bending. This change in shape and size increases the contact area between the awn and soil, increasing the total friction between the pile and the soil. Since surface friction of the geosystem and soil resists tensile uplift forces, more differential deployment along the vertical axis of the awn would increase the relative vertical projected area of the awn structure in the soil. For geosystems loaded in tension, the tension capacity is a key design driver for the foundation sizing requirements. Awn deployment has significant potential to increase tension capacity due to increased friction between the pile and the soil due to larger soil-structure contact area along the awns and larger vertical projected area of the structure leading to increase mobilization of soil volume and shearing area. The awns were developed using a parametric model (Tucker and Sychterz, 2022). This model provided control of the dimensions and arrangements of the awns. At this scale, the geosystems were printed monolithically so the awn was smoothly attached to the pile. Experimental testing utilized a polymer for the prototype and ease of construction for small specimens. Structural analysis was confirmed for the polymer structure and extended in this paper to analyze the behavior of steel

geosystems at small scale.

2. Equivalent stiff through bar-and-hinge model in dynamic relaxation

Stability of the bar-and-hinge model for origami requires a fold stiffness between panels and bend stiffness across the panel according to Sychterz and Baruah (2021). The method of dynamic relaxation (DR) proposed by Otter (1965) and Day (1965) a vector-based pseudo-dynamic analysis that does not require matrix inversion and results in a static solution. The purpose of this method is to solve for form-finding and element forces in a structure. To improve convergence, Barnes (1977; 1999) modified the method to include kinetic damping. This method has been used for decades in the design of membrane structures and cable stayed bridges (Barnes, 2013; Bel Hadj Ali et al., 2011).

Force exerted by folding stiffness, F_{FKi}, is the force resisting rotation due to folding stiffness at a node, i, and a similar equation exists for bending stiffness, F_{BKi}. This angle force is distributed to the elements that connect to current node i, proportional to their length. This model is developed to represent the steel awns protruding from the pile, to quantify the in-plane and out-of-plane deformation behavior. Fig. 2 describes the detailed steps for the creation of this model. Initially, the awns are analyzed to calculate the in-plane and out-of-plane deformations when loads are applied with pinned and roller boundary conditions. The loads are distributed across the end node. Fig. 3 shows the finite element model in SAP2000 of the awn for in-plane deformation on the short side (a) and out-of-plane deformation (b). In-plane model was simply supported, and the out-of-plane model was pinned at the corners. The force exerted on the awns was the experimentally derived initial actuation force of the awns within the soil medium of 12.2 N.

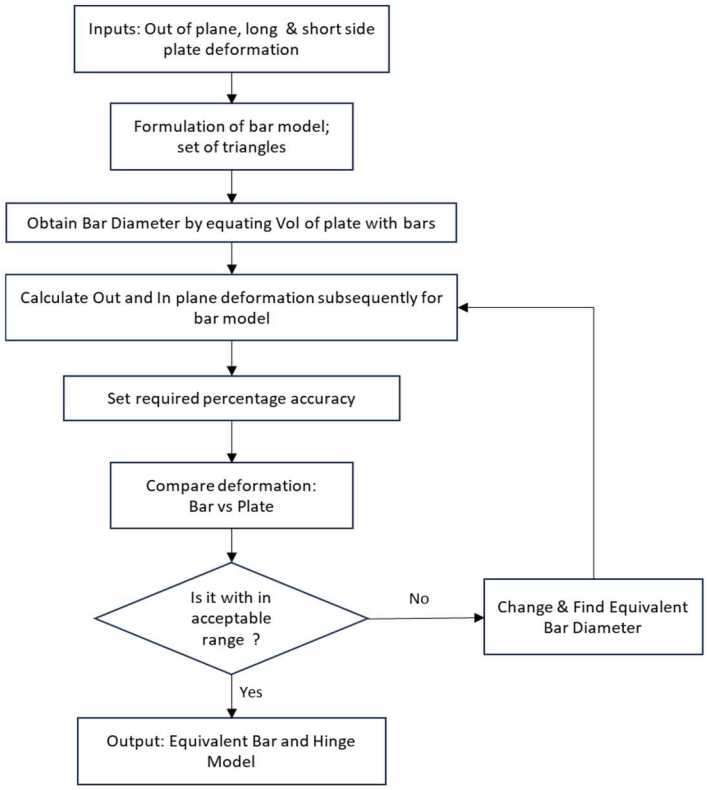

Figure 2: *Procedure for calculating equivalent bar area for thick origami.*

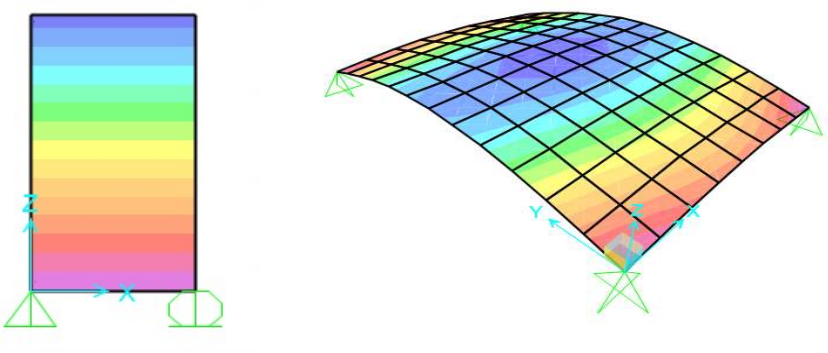

(a) In-plane Short Side (b) Out-of-plane

Figure 3*: Finite element model deformation results for in-plane (a) and out-of-pane (b) deformation of an awn.*

Awn deformation results from the finite element model using SAP2000 are shown in Table 1. The Young's Modulus for the awns was 29 GPa. With the same planar dimensions and thickness as the polymer awns, it is expected that the deformation is small at this scale. In-situ soil confinement will be greater than that of the small-scale tests and thus will be subject of future stability investigation.

Table 1: Actual Awn deformation

Test	Arc Length (mm)	Height (mm)	Thickness (mm)	Force (N)	Deformation (mm)
Out of plane	25.00	35.00	2.00	12.2	0.000102
In-plane Long Side	25.00	35.00	2.00	12.2	0.000042
In-plane Short side	25.00	35.00	2.00	12.2	0.000021

2. Formulation of Bar model

An equivalent bar model is created to represent the structural behavior of the awn. This model consists of pin-jointed circular bars connected by shared nodes. The bar elements are sized to match the overall geometry of the awn plate with 35 mm length, 25 mm height. To determine the individual bar diameters, the total volume of the steel in the awn plate is equated to the combined volume in all the circular bars as shown by the equation. This establishes an initial proportional size estimate across the various truss elements.

2.1 Out-of-plane deformations

With the initial bar model established, the out-of-plane deformations under loading are calculated and compared to the awn deformations. If the bar deformation results are within 10% confidence interval to the finite element model of the awn, then they are considered acceptable. If the error exceeds the 10% confidence interval, the stiffness of the bars is modified by adjusting their diameters. As shown in Fig. 4, a multiplier ratio is calculated between the bar model deformation and the target awn deformation. This ratio is then used to alter the bar diameters to better match stiffness. The out-of-plane deformation with the new diameters is re-calculated and compared to the experimental awn deformation. This iterative diameter tuning process is repeated until the bar model deformation is within 10% error margin of the measured awn values.

2.2 In-plane deformations

Using the tuned diameters from the out-of-plane analysis, the bar model is further assessed for in-plane deformations. Both the longitudinal and lateral axial deformations are quantified under

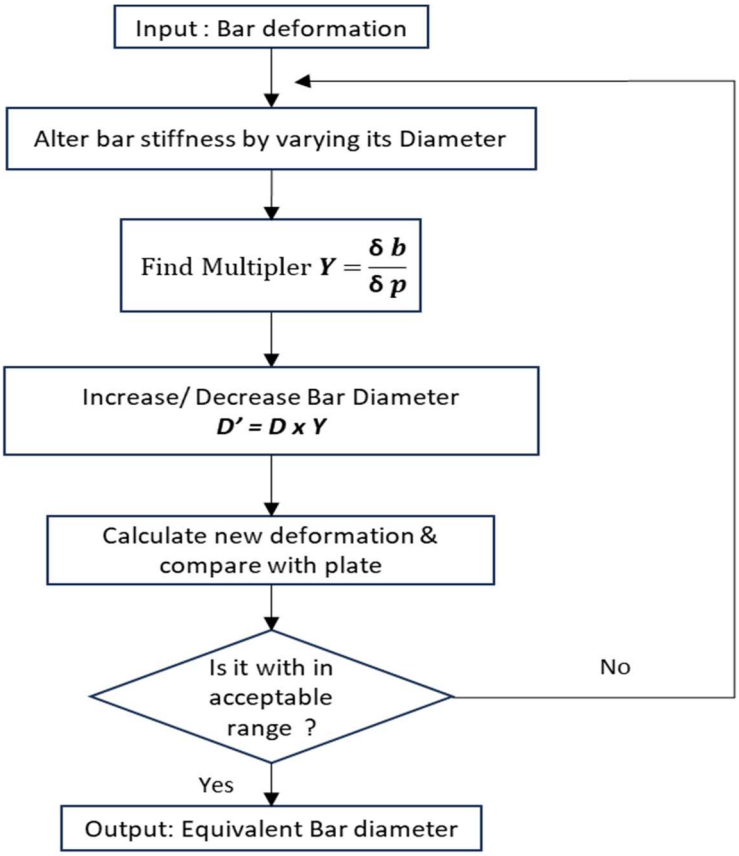

Figure 4: *Procedure for determining equivalent bar diameter for flexure.*

loading. These results are compared to the awn deformation. If the bar in-plane deformations match within 10% error margin, the model sufficiently represents an equivalent simulation of the awn. If deviations exceed 10%, the iterative diameter tuning process (Fig. 4) is repeated. The multiplier ratio continues modulating the bar diameters until alignment with awn in-plane deformations. The final optimal diameter proportions between the cross, short, and long bar elements are formulated as presented in Table 2. This ratio relationship enables scaled modeling of multi-awn pile systems in the future.

Table 2: Bar diameter ratio

Long Bar	Short Bar	Cross Bar
1.00	3.25	5.00

3. Analysis using dynamic relaxation

With the tunes and optimized bar and hinge model established, dynamic relaxation techniques are applied to simulate the deployment process. The same model geometry, loads, and boundary constraints are implemented as shown in Fig. 5(a) and 4(b). The in-plane deformation results from dynamic relaxation agree with the values predicted by the equivalent static bar and hinge model,

as highlighted in the summary table. This validates the in-plane representation. However, some discrepancy is noted for out-of-plane deformations from the dynamic analysis. Further refinement accounting for complex bend and fold angle effects would be required to improve correlation.

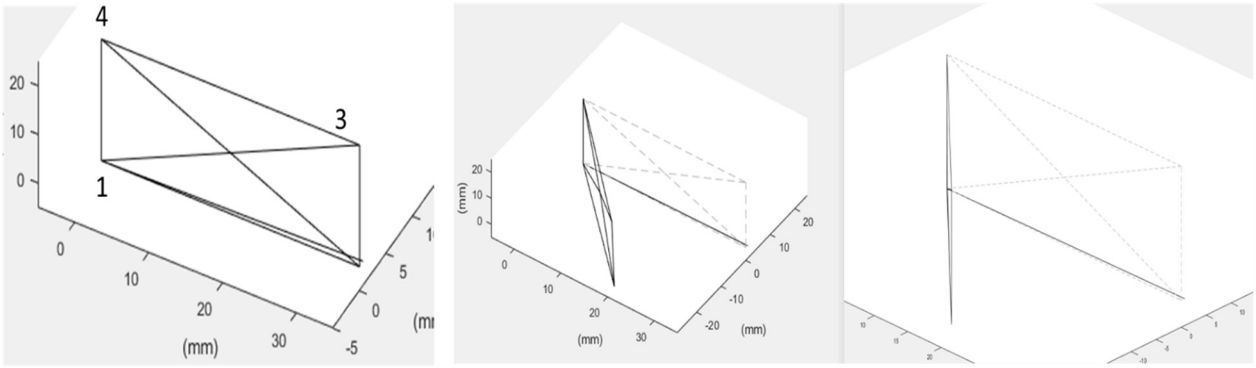

(a) In-Plane (b) Out-of-Plane

Figure 5: *Results from dynamic relaxation for awn deformation In-Plane and Out-of-Plane.*

4. Experimental testing

A document camera was positioned so that the curved edge of the awn was visible. The tension tests were performed by loading the awn with 10 N of force, unloading it, and then repeating the process for a total of three tests. This process was repeated with the camera facing the other side of the awn. For all models, the tests for the bottom of the awn were performed before the tests for the top of the awn.

For both the deployment and the tension tests, the video output and force output were synchronized to ensure that the force was known for any frame of the video. During testing, the video data was recorded by the native Windows Camera application and force data was recorded by PASCO Capstone software. Both windows were screen-recorded with Open Broadcasting Software (OBS) Studio to ensure that the outputs could later be synchronized. Data from the deployment tests was extracted by exporting two images of the deployment video – one before deployment and one at the maximum force. The forces at these frames were read from the synchronization video and noted. Each awn had a set of position trackers embedded into the print in the polymer prototype material (Fig. 6). A rotation tracker was also embedded into the pile.

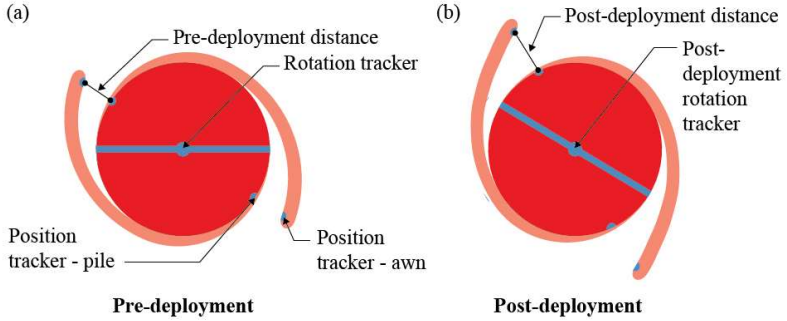

Figure 6: *Representation of trackers at pre-deployment (a) and post-deployment (b).*

In Rhinoceros 7, a 3D modelling software, distances between the position tracker located on the shell-like awn structure and the position tracker located on the pile were measured before and after deployment. This deployment distance was measured for each awn. The change in angle between

the pre-deployment and post-deployment rotation tracker was also found.
A similar method was used for the tension tests. Images were extracted for the pre-deployment state and each post-deployment state – defined here as the first frame where a force was recorded above 10 N. The curves were traced in Rhinoceros 7 and a composite curve was calculated for the three post-deployment states by finding the arithmetic mean of the three curves.

5. Embodied energy, material, and stability

A material analysis was carried out on the three tested awn arrangements along with a baseline pile without awns (Fig 7). When increased capacity is required for anchor piles, friction is increased by increasing the radius – and thus the surface area – of the piles. However, by comparing the designed geosystems and equivalent piles with identical surface areas, it is possible to compare the material usage of the two systems.

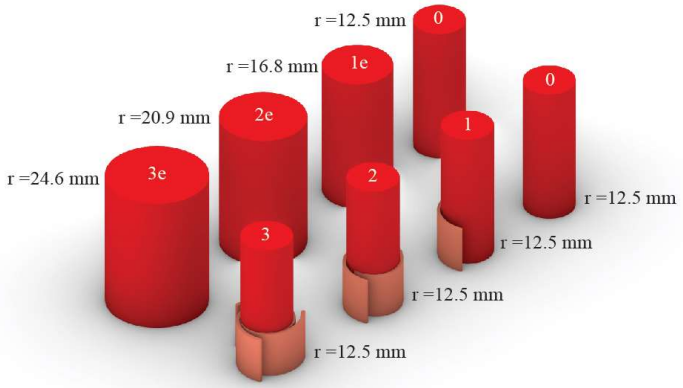

Figure 7: *Material analysis of tested geosystems and their pile-only counterparts.*

The surface area of each geosystem was calculated in Rhinoceros 7 and a pile with an equivalent surface area and height was generated. The volume of each geosystem and equivalent pile was calculated and compared (Table 3).

Table 3: *Surface area and volume for tested geosystems and equivalent piles.*

Type	Radius (mm)	Height (mm)	Surface Area (cm^2)	Volume (cm^3)
Baseline	12.5	75.0	69	37
1 Awn Geosystem	12.5	75.0	97	38
1 Awn Pile-Only	16.8	75.0	97	67
2 Awn Geosystem	12.5	75.0	126	40
2 Awn Pile-Only	20.9	75.0	126	102
3 Awn Geosystem	12.5	75.0	154	42
3 Awn Pile-Only	24.6	75.0	154	143

Through this analysis, it was determined that a geosystem comprised of deployable compliant awns attached to a cylindrical pile uses less material than an equivalent anchor pile. While all the

geosystems were more materially efficient than their pile-only counterparts, the effect of adding each additional awn was more pronounced. A one-awn geosystem provided a 42% reduction in material in comparison to a pile-only system with identical surface area. For a two-awn geosystem, this reduction increased to 61% and for a three-awn geosystem, the reduction in material was 71%. The difference in the material reduction effect is largest between a one-awn system and a two-awn system. Adding additional awns correlates with increased deployment force, but this effect should be considered in combination with the volume of material used and with the practicalities of construction. The deployment force is an indicator of the ease of installation but may also be a predictor for tensile capacity. Fig. 8 illustrates the conceptual relationship between required force and stiffness.

When awns are difficult to deploy, they also may be difficult to pull out of soil – increasing the tensile capacity of the geosystem. A higher deployment force – which may predict higher tensile capacity – can be helpful. However, it may not be feasible to install a geosystem that has an extremely high deployment force. Too low or too high of a deployment force impact stability of the geosystem. Balancing the desire for higher tensile capacity with the reality of needing to deploy the awns in a construction environment leads to a two-awn geosystem as an ideal trade-off between resistance and amount of material used.

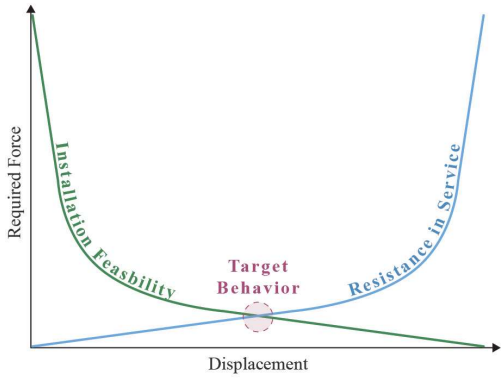

Figure 8: *Representation of relationship between required force and stiffness, showing resistance in service (green), installation feasibility (blue), and target behavior (pink).*

4. Conclusions

Dynamic relaxation method can be successfully harnessed to model thick origami to assess the stability of the steel system by correlating awn deformations through an iterative model tuning process, the truss element diameters were optimized to within the desired accuracy. Stiffness from the bend and fold angles enhanced out-of-plane correlation. The established modeling approach and the validated truss representation can enable examining geosystems at a larger scale and multi-awn systems.

Acknowledgments

Support from the National Science Foundation (CMMI_2207296), the University of Illinois at Urbana-Champaign, and the State of Illinois are gratefully acknowledged.

References

Pellegrino, S. (2001) "Deployable Structures." *Wien-New York: Springer Verlag.*

Akgün, Y., Gantes, C., Sobek, W., Korkmaz, K., and Kalochairetis, K. (2011) "A novel adaptive spatial scissor-hinge structural mechanism for convertible roofs," *Engineering Structures*, vol. 33, no. 4, 1365–1376.

García-Mora, C.J., and Sánchez-Sánchez, J. (2021) "Actuation methods for deployable scissor structures," *Automation in Construction*, vol. 131, p. 103894.

Furuya, H. (1992). "Concept of Deployable Tensegrity Structures in Space Application," *International Journal of Space Structures*, vol. 7, no. 2, 143–151.

Tibert, G. (2002). "Deployable Tensegrity Structures for Space Applications," *Royal Institute of Technology*.

Block, J., Straubel, M., and Wiedemann, M. (2011). "Ultralight deployable booms for solar sails and other large gossamer structures in space," *Acta Astronautica*, vol. 68, no. 7, 984–992.

Tibert, G. and Pellegrino, S. (2003). "Deployable Tensegrity Masts," *44th AIAA/ASME/ASCE/AHS/ASC Structures, Structural Dynamics, and Materials Conference.*

Datashvili, L., Baier, H., Wehrle, E., Kuhn, T., and Hoffmann, J. (2010). "Large Shell-Membrane Space Reflectors," *51st AIAA/ASME/ASCE/AHS/ASC Structures, Structural Dynamics, and Materials Conference
 18th AIAA/ASME/AHS Adaptive Structures Conference*, Orlando, Florida: American Institute of Aeronautics and Astronautics.

Howell, L.L., Magleby, S.P., and Olsen, B.M. (2013). "Handbook of compliant mechanisms". Chichester, West Sussex, United Kingdom Hoboken, New Jersey: *John Wiley & Sons*, Inc.

Kota, S., Joo, J., Li, Z., Rodgers, S.M., and Sniegowski, J. (2001). "Design of Compliant Mechanisms: Applications to MEMS," *Analog Integrated Circuits and Signal Processing*, vol. 29, no. 1, 7–15.

Kota S. and Ananthasuresh, G.K. (1995). "Designing compliant mechanisms," *Mechanical Engineering-CIME*, vol. 117, no. 11, 93–97.

Frecker, M. (2013). "Synthesis through Topology Optimization," *Handbook of Compliant Mechanisms*, John Wiley & Sons, Ltd, 93–107.

Zentner, L., and Böhm, V. (2009). "On the Classification of Compliant Mechanisms," *Proceedings of EUCOMES 08, M. Ceccarelli*, Ed., Dordrecht: Springer Netherlands, 431–438.

Howell, L.L. (2013). "Introduction to Compliant Mechanisms," *Handbook of Compliant Mechanisms*, John Wiley & Sons, Ltd, 1–13.

Aubeny, C. (2017). "Geomechanics of Marine Anchors. Boca Raton", *CRC Press*, doi: 10.4324/9781351237376.

Colaço, A., Alves Costa, P., Mont'Alverne Parente, C., and Silva Cardoso, A. (2021). "Ground-borne noise and vibrations in buildings induced by pile driving: An integrated approach," *Applied Acoustics*, vol. 179, p. 108059.

Prasad, Y., and Rao, S.N. (1996) "Lateral Capacity of Helical Piles in Clays," *Journal of Geotechnical Engineering*, vol. 122, no. 11, 938–941.

Tom, J., O'Loughlin, C., White, D., Haghighi, A., and Maconochie, A. (2017). "The effect of radial fins on the uplift resistance of buried pipelines," *Géotechnique Letters*, vol. 7.

Wilde, B., Treu, H., and Fulton, T. (2001). "Field Testing of Suction Embedded Plate Anchors," *The Eleventh International Offshore and Polar Engineering Conference*, OnePetro.

Sakr, M., Nazir, A., Azzam, A., and Sallam, A. (2020). "Model study of single pile with wings under uplift loads," *Applied Ocean Research*, vol. 100, p. 102187.

Lienhard, J., Schleicher, S., and Knippers, J. (2015). "Bio-inspired, Flexible Structures and Materials," *Biotechnologies and Biomimetics for Civil Engineering.*

Vincent, J. F. V. (2003). "Deployable Structures in Biology," *Morpho-functional Machines: The New Species*.

Baerlecken, D., Gentry, R., Swarts, M., and Wonoto, N. (2014). "Structural, Deployable Folds — Design and Simulation of Biological Inspired Folded Structures*," International Journal of Architectural Computing*, vol. 12, no. 3, 243–262.

Sychterz, A.C., Bernardi, I., Tom, J.G., and Beemer, R.D. (2021). "Nonlinear soil-structure behavior of a deployable and compliant anchor system," *Canadian Journal of Civil Engineering*. 1-10

Tucker, K., and Sychterz, C.A., (2022). “Analyzing Geosystems with Deployable Compliant Mechanisms for Enhanced Tension Capacity*,” Proceedings of the Canadian Society of Civil Engineering Annual Conference 2022*.

Otter, J. (1965). “Computations for prestressed concrete reactor pressure vessels using dynamic relaxation.” *Nuclear Structural Engineerin*g 1, 61–75.

Day, A.S. (1965). “An introduction to dynamic relaxation (dynamic relaxation method for structural analysis, using computer to calculate internal forces following development from initially unloaded state).” *The Engineer* 219, 218–221

Barnes, M. (1977). “Form-finding and analysis of tension space structures by dynamic relaxation.” Ph.D. thesis. *City University.*

Barnes, M. (1999). “Form finding and analysis of tension structures by dynamic relaxation*”. International journal of space structures* 14, 89–104.

Barnes, M.R., Adriaenssens, S., Krupka, M. (2013). “A novel torsion/bending element for dynamic relaxation modeling.” *Computers & Structures* 119, 60–67.

Bel Hadj Ali, N., Rhode-Barbarigos, L., Smith, I. (2011). “Analysis of clustered tensegrity structures using a modified dynamic relaxation algorithm.” *International Journal of Solids and Structures* 48, 637–647.